

Mutual Contrastive Learning to Disentangle Whole Slide Image Representations for Glioma Grading

Lipei Zhang¹, Yiran Wei², Ying Fu³, Stephen Price², Carola-Bibiane Schönlieb¹, and Chao Li ^{*1,2}

¹ Department of Applied Mathematics and Theoretical Physics, Cambridge, UK

² Department of Clinical Neurosciences, University of Cambridge, UK

³ School of Computer Science and Technology, Beijing Institute of Technology

Abstract. Whole slide images (WSI) provide valuable phenotypic information for histological assessment and malignancy grading of tumors. The WSI-based computational pathology promises to provide rapid diagnostic support and facilitate digital health. The most commonly used WSI are derived from formalin-fixed paraffin-embedded (FFPE) and frozen sections. Currently, the majority of automatic tumor grading models are developed based on FFPE sections, which could be affected by the artifacts introduced by tissue processing. Here we propose a mutual contrastive learning scheme to integrate FFPE and frozen sections and disentangle cross-modality representations for glioma grading. We first design a mutual learning scheme to jointly optimize the model training based on FFPE and frozen sections. Further, we develop a multi-modality domain alignment mechanism to ensure semantic consistency in the backbone model training. We finally design a sphere normalized temperature-scaled cross-entropy loss (NT-Xent), which could promote cross-modality representation disentangling of FFPE and frozen sections. Our experiments show that the proposed scheme achieves better performance than the model trained based on each single modality or mixed modalities. The sphere NT-Xent loss outperforms other typical metrics loss functions.

Keywords: Glioma · Whole slide image · Digital pathology · Contrastive learning · Representation Disentangling.

1 Introduction

Glioma is the most frequent malignant primary brain tumor, characterized by remarkable infiltration and tumor heterogeneity [26,13,14]. According to the World Health Organization (WHO) classification, glioma is classified into four grades, where grade IV represents the most aggressive type, and lower grade glioma (LGG), i.e., grades II and III, are less aggressive [13,14].

* Corresponding author

Glioma grading is of crucial significance for treatment planning and risk stratification towards precision medicine [24,12,11]. The current practice of glioma grading is based on the histology assessment of tumor specimens, which is time-consuming and requires high professional expertise. Therefore, an accurate and automatic approach of glioma grading based on the whole slide images (WSI) acquired from the specimen promises to provide rapid diagnostic support for timely clinical decision making. Furthermore, a computer-assisted method could help facilitate digital health and enhance the accessibility of medical resources.

Two types of WSI are available depending on the procedure of tissue sectioning. The FFPE tissue section is used as the diagnostic standard in clinical practice, which is time-consuming in processing tissue. Importantly, the artifacts introduced by formalin can affect the interpretation of histological specimens [15]. Specifically, the procedure of prefixation and fixation could influence the morphological quality of FFPE specimens [2]. These artifacts pose particular challenges to the model training based on WSI.

In parallel, frozen sections provide a rapid approach of tumor grading to guide intra- or peri-operative clinical decisions. Although frozen sections typically contain limited tissue, the sample hydration and cellular morphology of the frozen tissue can be preserved at a natural state [5], which may provide crucial information for tumor grading. Hence, the frozen sections could provide important complementary information to the FFPE sections for tumor grading.

Here we hypothesise that integrating FFPE and frozen sections could train a more robust model to learn the high-level representations reflecting tumor malignancy, with less bias from the artefacts caused by tissue processing. We design a parallel mutual learning scheme to facilitate the integration of FFPE and frozen sections in model training. We adopt the domain alignment approach to achieve semantic consistency in model training to adjust the multi-modality input. We further design a sphere NT-Xent to disentangle representation with the sphere projection [8].

To our best knowledge, this is the first cross-modality mutual contrastive learning approach for glioma grading in the field of digital pathology. Our contributions include:

- a mutual learning scheme for joint optimisation of model training based on the WSIs of FFPE and frozen sections.
- a domain alignment mechanism across FFPE and frozen sections based on sampling without replacement to ensure semantic consistency.
- a sphere NT-Xent loss to improve the ability to disentangle cross-modality representations in the mutual learning process.

2 Related work

Modelling WSI remains challenging due to the gigapixel size of the images and the complexity of tumor tissue. To mitigate the challenge of computational costs, multiple instance learning (MIL) is used as an effective method in model training [10,21]. Using MIL, previous studies proposed machine learning approaches based

on feature engineering [22,18]. Although providing reasonable performance, these approaches were prone to model generalizability due to the less robust features extracted from heterogeneous tumor tissue. Recently, deep learning has achieved superior performance using the end-to-end training scheme. Most state-of-the-art models employed the transfer learning approach to transfer the pre-trained weights from ImageNet [10,6,19,21]. Based on the FFPE sections, these studies might be affected by the bias from FFPE tissue. Moreover, a single section modality may not facilitate learning relevant image representations for tumor grading.

Recent studies show that collaborative learning is capable of extracting common features from natural and medical images [27,23]. In addition, domain alignment [17,29] and the contrastive loss [4,23] can further promote the network in extracting more precise features in the collaborative learning. Based on these methods, a cross-modality mutual learning scheme becomes feasible, which could outperform the single modality training.

3 Methods

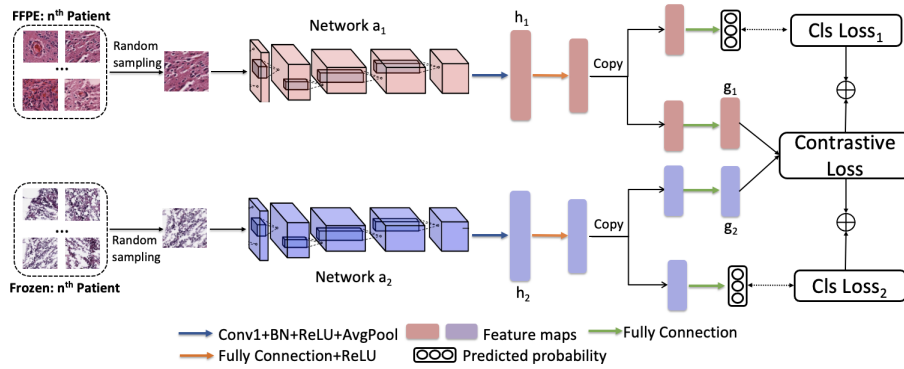


Fig. 1. The pipeline of gliomas grading on FFPE section and frozen section.

The proposed parallel mutual learning scheme is shown in Fig. 1, which is based on mutual optimisation learning. Initially, a multi-modality domain alignment strategy is proposed for data sampling before training. The paired images are input into the Network α_1 and α_2 , respectively. In each branch, the set of feature vectors (h_1 and h_2) after first fully connection and ReLU are copied into the multi-heads. One head is for classification, and the other is designed to achieve representation disentangling across the modalities. Combining classification loss and contrastive loss could optimize each branch via the back-propagation. We introduce details of the main design in the following.

Multi-modality domain alignment. This design describes the introduction of loading data from two different data types. For a given patch sampled from n_{th} patient FFPE bag, the other patch from n_{th} is randomly sampled without replacement. This operation can ensure the multi-modality domain alignment, allowing semantic consistency across patients to follow the procedure.

Multi-heads. We adopt multi-heads in our scheme to promote better projection of latent vectors for different functions. In each modal network, the latent vectors after average pooling are transformed by first fully connection and copied into two heads respectively for two tasks. One head is used for down-sampling the latent vectors to predict tumor grades. The other head includes a hidden layer with the same dimension, such that we can obtain a representative vector after the non-linear projection ($z_i = g(h_i) = W^2\sigma(W^1h_i)$), where σ is a ReLU non-linearity. Referred by the experiments of SimCLR [4], a non-linear operator can remove variant information, e.g., the color or orientation of objects resulting from various staining procedures from multiple centers. Therefore, the classification head can leverage the nonlinear transformation to maintain more useful information in h , which could boost the performance.

Sphere NT-Xent loss. For this design, we firstly view the FFPE and the frozen section images as images sampled from different augmented views on the same patient. In standard contrastive loss definition presented in [4,9], l_2 normalization was used for reference and augmented images. However, the image pairs used in self-supervised learning keep unified features and distribution, and l_2 normalization can scale latent vector into a valid range. In our task, the image pairs include two domains with different distributions. Therefore, we adopt layer normalization, as shown in Eq. 1, to center and rescale the latent space into the same sphere, which can improve the efficiency of disentangling.

$$\hat{g}_n = \frac{g_n - \mu_n}{\sqrt{(\sigma_n)^2 + \epsilon}} \quad (1)$$

where $n \in \{1, 2\}$ and g_n denotes the latent vector from FFPE or frozen section. μ and σ are mean and variance of each batch. Moreover, we denote $sim(\hat{g}_1, \hat{g}_2) = \frac{\hat{g}_1^T \hat{g}_2}{\|\hat{g}_1\| \cdot \|\hat{g}_2\|}$ as the cosine similarity between \hat{g}_1 and \hat{g}_2 . The Sphere NT-Xent loss function can be defined as:

$$L_{contrastive} = -\log \frac{\exp(sim(\hat{g}_a, \hat{g}_b)/\tau)}{\sum_{i \in I} \mathbb{1}_{i \neq b} \exp(sim(\hat{g}_a, \hat{g}_i)/\tau)} \quad (2)$$

where $\mathbb{1}_{i \neq b} \in \{0, 1\}$ is an indicator, which values $\mathbb{1}$ only when $i \neq b$. We also define τ as a temperature hyper-parameter.

Optimisation Model. Our learning scheme consists of two functions to achieve joint optimisation in two classification tasks. Each function consists of a cross-entropy (CE) loss with Taylor Softmax [7], and a contrastive loss. The Taylor Softmax CE can be formed as Eq. 3 and total loss function of each model

can be expressed as Eq. 4:

$$L_{cls}(f(x), y) = \sum_{i=1}^t \frac{(1 - f_y(x))^i}{i} \quad (3)$$

$$\begin{aligned} L_{FFPE} &= L_{cls_1} + L_{contrastive} \\ L_{frozen} &= L_{cls_2} + L_{contrastive} \end{aligned} \quad (4)$$

4 Experimental Setup

4.1 Datasets

We utilised the WSI of glioblastoma (GBM) and LGG from the Cancer Genome Atlas (TCGA) dataset [1], with clinical details and Hematoxylin and Eosin (HE) stained sections available. We only selected 499 patients (201 grade II, 229 grade III and 119 grade IV) with both FFPE and frozen sections available.

For data pre-processing, we designed three steps: 1) transforming a low-dimension version of WSI into HSV color space and separating HE-stained tissue from the background using Otsu’s Binarization on the saturation channel [3]; 2) patching a number of non-overlapping 500×500 instance-level images at $20\times$ magnification; 3) a blob detection procedure [25] to further remove redundant patches containing insufficient tissue. The numbers of finally included patches were 1,680,714 for FFPE sections and 483,886 for frozen sections.

To evaluate the proposed scheme, the dataset was randomly divided into 349 patients for the training set, 50 patients for the validation set and 100 patients for the testing set. Moreover, to increase sample size, we cropped sub-regions of patches into a size of 224×224 . In addition, we applied data augmentation techniques (random rotation of 90° , 180° , 270° , random flipping image along axis, shift hue saturation value and brightness contrast) to increase the training sample size.

4.2 Training Details

The training environment was based on PyTorch 1.6.0 backend with acceleration by Nvidia RTX 3090. The batch size was set to 128, corresponding to 128 pairs of FFPE and frozen images in the mutual training, while 128 of FFPE or frozen images in single training and mixed training. The input was $224 \times 224 \times 3$. We used the loss function described in. Eq.4 for our experiments. The number of training epochs was 10, and the optimizer was Adam with default parameters. Cosine annealing warm restarts were adopted with an initial learning rate of 1.6×10^{-4} .

We trained different CNN backbones with single input training (baseline) [10,21], mixed training, mutual training scheme. We compared the performance of different contrastive loss in mutual training such as Kullback-Leibler divergence [27], marginal triplet loss [20], NT-logistic loss and NT-loss [4].

4.3 Testing Details

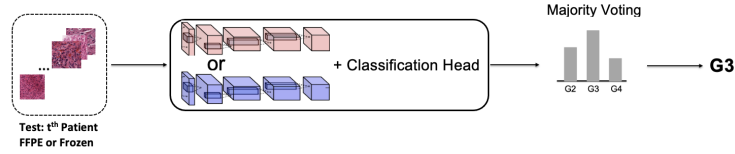


Fig. 2. The pipeline of gliomas grading on FFPE section and frozen section.

The details of the inference phase are shown in Fig. 2. FFPE and frozen sections are classified separately by Network a_1 or a_2 with respective classification heads. After predicting all images in a patient’s bag, the number of predicted grades is counted by the histogram and majority voting is used to determine the final predicted tumor grade.

5 Results

5.1 Quantitative Results

Table 1. Comparison with different learning schemes and backbones

		FFPE			frozen		
		Accuracy	Precision	Recall	Accuracy	Precision	Recall
EfficientNet-B0	Baseline	0.69	0.70	0.69	0.65	0.67	0.65
	Mixed training	0.71	0.72	0.71	0.61	0.70	0.61
	Mutual training	0.75	0.77	0.75	0.72	0.75	0.72
ResNet50	Baseline	0.68	0.68	0.68	0.65	0.70	0.70
	Mixed training	0.71	0.68	0.68	0.68	0.70	0.70
	Mutual training	0.77	0.76	0.76	0.73	0.71	0.72

For comparison, the evaluation metrics on different CNN backbones with single input training, mixed training and mutual training scheme are shown in Table 1. We chose EfficientNet-B0 and ResNet50 to evaluate the model performance in these experiments. We observe that our proposed learning scheme outperforms the single and mixed training on the given backbone from the experiments. These results suggest that the performance of the single training could be limited by the information from each single specific modality, while the mixed training may not efficiently obtain complementary information from the batch-size learning. After being applied on the different backbone networks, the mutual learning scheme demonstrates the capability of disentangling mutual information in the same latent vector space, which could increase the model performance.

5.2 Visualization

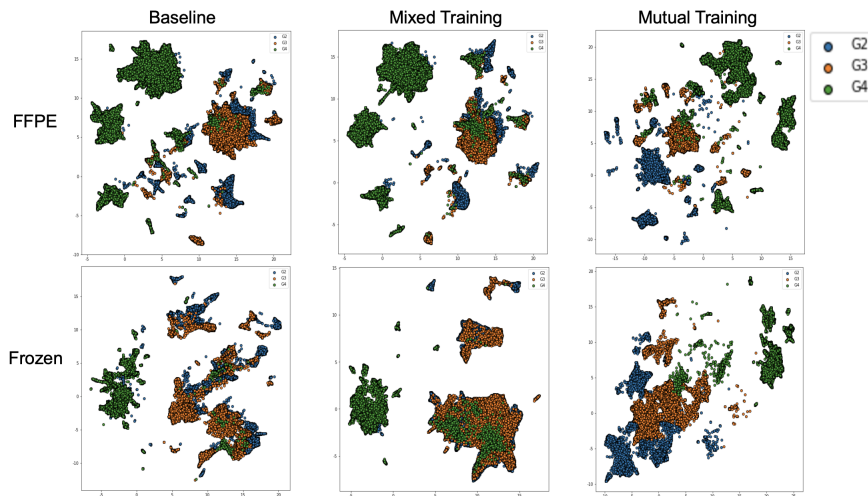


Fig. 3. Mutual learning scheme interpretability in brain tumor grading. Each point is from reducing dimension of the latent vector by UMAP method.

Table 2. Comparison with different metrics loss functions

	FFPE			frozen		
	Accuracy	Precision	Recall	Accuracy	Precision	Recall
KL-loss	0.71	0.70	0.68	0.71	0.68	0.69
Marginal triplet loss	0.73	0.70	0.71	0.72	0.68	0.72
NT-Logistic loss	0.74	0.74	0.72	0.71	0.68	0.70
NT-Xent	0.75	0.74	0.74	0.71	0.70	0.69
Sphere NT-Xent	0.77	0.76	0.76	0.73	0.76	0.73

To further demonstrate that our proposed sphere NT-Xent could fulfil a better representation disentangling, we compared with other loss functions as shown in Table. 2. We observe that the NT-Xent loss provides superior performance, benefiting the representation of Disentangled Learning. In comparison, KL-loss fails to consider the distance between positive and negative samples, which might lead to worse performance than other loss functions. As for the marginal triplet and NT-logistic loss, they are measured using the absolute similarity of the positive and negative samples. By contrast, the NT-Xent loss is calculated using the relative similarity, which may help the network optimize the balance between separating the samples of different classes while maintaining the overall model

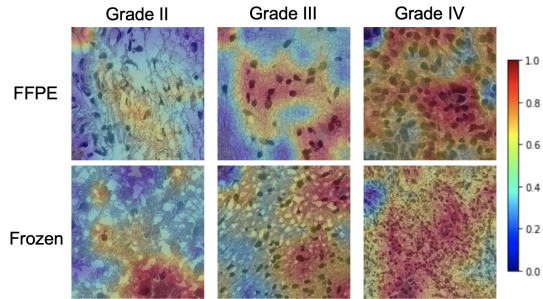


Fig. 4. Image-level predicted heatmap of three tumor grades by mutual learning. Left to right: Grade II, III, and IV). The FFPE and Frozen images of each grade are from the same patients. The color bar indicates the estimated level of attention on the region.

generalization. Moreover, the results illustrate that the sphere projection, provided by the layer normalization, improves the mutual information disentangling, compared with the original NT-Xent loss.

To understand how a mutual learning scheme leverages representation disentangling in predicting tumor grades, we visualized the latent vector from single training, mixed training and mutual training on FFPE and frozen section images, using the Uniform Manifold Approximation and Projection (UMAP) method [16]. As shown in Fig. 3, the latent vectors are obtained from the CNN extractors. The results show that the mutual training scheme could promote representation disentangling, which may help the latent vector on the classification head preserve more helpful information from the same tumor grade, demonstrating closer distribution in the feature space.

The qualitative performance of the randomly selected statistical features from the mutual learning is illustrated in Fig. 4. These salient maps are generated by classification activation maps (CAMs) [28]. The examples in Fig. 3 show that the trained model by the mutual learning can focus on the proliferation region, which helps efficiently detect tissue morphology from the WSI.

6 Conclusions

We propose a mutual contrastive learning scheme to improve the performance of glioma grading based on whole slide images. We first develop a mutual learning scheme to extract relevant image representations by integrating FFPE and frozen sections with complementary information. Next, we employ a multi-modality domain alignment mechanism to maintain semantic consistency across the FFPE and frozen sections. We further design a sphere NT-Xent, which could promote cross-modality representation disentangling within the same sphere. We demonstrate that our learning scheme could mitigate the drawbacks of the training schemes based on a single modality or mixed modalities. Our experiments show that the sphere NT-Xent outperforms other typical metrics loss. The proposed

learning scheme may be generalised to tumor grading of different systems and other cross-modality learning tasks.

References

1. The cancer genome atlas. <https://tcga-data.nci.nih.gov/tcga/>
2. Bass, B.P., Engel, K.B., Greytak, S.R., Moore, H.M.: A review of preanalytical factors affecting molecular, protein, and morphological analysis of formalin-fixed, paraffin-embedded (ffpe) tissue: how well do you know your ffpe specimen? *Archives of pathology and laboratory medicine* **138**(11), 1520–1530 (2014)
3. Chen, R.J., Lu, M.Y., Shaban, M., Chen, C., Chen, T.Y., Williamson, D.F., Mahmood, F.: Whole slide images are 2d point clouds: Context-aware survival prediction using patch-based graph convolutional networks. In: *International Conference on Medical Image Computing and Computer-Assisted Intervention*. pp. 339–349. Springer (2021)
4. Chen, T., Kornblith, S., Norouzi, M., Hinton, G.: A simple framework for contrastive learning of visual representations. In: *International conference on machine learning*. pp. 1597–1607. PMLR (2020)
5. Cohen, M., Varki, N.M., Jankowski, M.D., Gagneux, P.: Using unfixed, frozen tissues to study natural mucin distribution. *JoVE (Journal of Visualized Experiments)* (67), e3928 (2012)
6. Deng, J., Dong, W., Socher, R., Li, L.J., Li, K., Fei-Fei, L.: Imagenet: A large-scale hierarchical image database. In: *2009 IEEE conference on computer vision and pattern recognition*. pp. 248–255. Ieee (2009)
7. Feng, L., Shu, S., Lin, Z., Lv, F., Li, L., An, B.: Can cross entropy loss be robust to label noise? In: *Proceedings of the Twenty-Ninth International Conference on International Joint Conferences on Artificial Intelligence*. pp. 2206–2212 (2021)
8. Guo, J., Chen, M., Hu, Y., Zhu, C., He, X., Cai, D.: Spherical knowledge distillation (2020)
9. He, K., Fan, H., Wu, Y., Xie, S., Girshick, R.: Momentum contrast for unsupervised visual representation learning. In: *Proceedings of the IEEE/CVF conference on computer vision and pattern recognition*. pp. 9729–9738 (2020)
10. Im, S., Hyeon, J., Rha, E., Lee, J., Choi, H., Jung, Y., Kim, T.: Classification of diffuse glioma subtype from clinical-grade pathological images using deep transfer learning. *Sensors* **21**(10), 3500 (2021)
11. Li, C., Wang, S., Liu, P., Torheim, T., Boonzaier, N.R., van Dijken, B.R., Schönlieb, C.B., Markowetz, F., Price, S.J.: Decoding the interdependence of multiparametric magnetic resonance imaging to reveal patient subgroups correlated with survivals. *Neoplasia* **21**(5), 442–449 (2019)
12. Li, C., Yan, J.L., Torheim, T., McLean, M.A., Boonzaier, N.R., Zou, J., Huang, Y., Yuan, J., van Dijken, B.R., Matys, T., et al.: Low perfusion compartments in glioblastoma quantified by advanced magnetic resonance imaging and correlated with patient survival. *Radiotherapy and Oncology* **134**, 17–24 (2019)
13. Louis, D.N., Ohgaki, H., Wiestler, O.D., Cavenee, W.K., Burger, P.C., Jouvett, A., Scheithauer, B.W., Kleihues, P.: The 2007 who classification of tumours of the central nervous system. *Acta neuropathologica* **114**(2), 97–109 (2007)
14. Louis, D.N., Perry, A., Reifenberger, G., Von Deimling, A., Figarella-Branger, D., Cavenee, W.K., Ohgaki, H., Wiestler, O.D., Kleihues, P., Ellison, D.W.: The 2016 world health organization classification of tumors of the central nervous system: a summary. *Acta neuropathologica* **131**(6), 803–820 (2016)

15. Mathieson, W., Thomas, G.A.: Why formalin-fixed, paraffin-embedded biospecimens must be used in genomic medicine: An evidence-based review and conclusion. *Journal of Histochemistry & Cytochemistry* **68**(8), 543–552 (2020)
16. McInnes, L., Healy, J., Melville, J.: Umap: Uniform manifold approximation and projection for dimension reduction. arXiv preprint arXiv:1802.03426 (2018)
17. Motiian, S., Piccirilli, M., Adjeroh, D.A., Doretto, G.: Unified deep supervised domain adaptation and generalization. In: Proceedings of the IEEE international conference on computer vision. pp. 5715–5725 (2017)
18. Mousavi, H.S., Monga, V., Rao, G., Rao, A.U.: Automated discrimination of lower and higher grade gliomas based on histopathological image analysis. *Journal of pathology informatics* **6** (2015)
19. Pei, L., Jones, K.A., Shboul, Z.A., Chen, J.Y., Iftekharuddin, K.M.: Deep neural network analysis of pathology images with integrated molecular data for enhanced glioma classification and grading. *Frontiers in oncology* **11**, 2572 (2021)
20. Schroff, F., Kalenichenko, D., Philbin, J.: Facenet: A unified embedding for face recognition and clustering. In: Proceedings of the IEEE conference on computer vision and pattern recognition. pp. 815–823 (2015)
21. Truong, A.H., Sharmanska, V., Limback-Stanic, C., Grech-Sollars, M.: Optimization of deep learning methods for visualization of tumor heterogeneity and brain tumor grading through digital pathology. *Neuro-Oncology Advances* **2**(1), vdaa110 (2020)
22. Wang, X., Wang, D., Yao, Z., Xin, B., Wang, B., Lan, C., Qin, Y., Xu, S., He, D., Liu, Y.: Machine learning models for multiparametric glioma grading with quantitative result interpretations. *Frontiers in neuroscience* p. 1046 (2019)
23. Wei, Y., Li, C., Chen, X., Schönlieb, C.B., Price, S.J.: Collaborative learning of images and geometrics for predicting isocitrate dehydrogenase status of glioma. arXiv preprint arXiv:2201.05530 (2022)
24. Wu, J., Li, C., Gensheimer, M., Padda, S., Kato, F., Shirato, H., Wei, Y., Schönlieb, C.B., Price, S.J., Jaffray, D., et al.: Radiological tumour classification across imaging modality and histology. *Nature Machine Intelligence* **3**(9), 787–798 (2021)
25. Xu, Y., Wu, T., Gao, F., Charlton, J.R., Bennett, K.M.: Improved small blob detection in 3d images using jointly constrained deep learning and hessian analysis. *Scientific reports* **10**(1), 1–12 (2020)
26. Zadeh Shirazi, A., McDonnell, M.D., Fornaciari, E., Bagherian, N.S., Scheer, K.G., Samuel, M.S., Yaghoobi, M., Ormsby, R.J., Poonnoose, S., Tumes, D.J., et al.: A deep convolutional neural network for segmentation of whole-slide pathology images identifies novel tumour cell-perivascular niche interactions that are associated with poor survival in glioblastoma. *British Journal of Cancer* **125**(3), 337–350 (2021)
27. Zhang, Y., Xiang, T., Hospedales, T.M., Lu, H.: Deep mutual learning. In: Proceedings of the IEEE conference on computer vision and pattern recognition. pp. 4320–4328 (2018)
28. Zhou, B., Khosla, A., Lapedriza, A., Oliva, A., Torralba, A.: Learning deep features for discriminative localization. In: Proceedings of the IEEE conference on computer vision and pattern recognition. pp. 2921–2929 (2016)
29. Zhu, X., Pang, J., Yang, C., Shi, J., Lin, D.: Adapting object detectors via selective cross-domain alignment. In: Proceedings of the IEEE/CVF Conference on Computer Vision and Pattern Recognition. pp. 687–696 (2019)